İSTANBUL UNIVERSITY CERRAHPAŞA

ORIGINAL ARTICLE
Electrica 2025; 25: 1-11

Modeling and Control of DC to High-Frequency AC Voltage Conversion for Photovoltaic Systems Under Variable Irradiation, Temperature and Load Conditions

Fatih Issi, Mustafa Karhan

Department of Computer Engineering, Engineering Faculty, Cankiri Karatekin University, Cankiri, Turkey

Cite this article as: F. Issi and M. Karhan, "Modeling and control of DC to high-frequency AC voltage conversion for photovoltaic systems under variable irradiation, temperature and load conditions," *Electrica*, 25, 0198, 2025. doi: 10.5152/electrica.2025.24198.

WHAT IS ALREADY KNOWN ON THIS TOPIC?

- *This study presents a dynamic control model integrating a Cuk Converter and a Class-E inverter regulated by a PI controller, which effectively maintains a stable 100V (RMS) AC output under varying irradiation, temperature, and load conditions in photovoltaic systems.*

WHAT THIS STUDY ADDS ON THIS TOPIC?

- *Photovoltaic (PV) panel output is significantly affected by environmental variables such as irradiation and temperature, requiring power conditioning methods to stabilize the voltage for reliable system operation.*

Corresponding author:
Fatih Issi

E-mail:
fatihissi@karatekin.edu.tr

Received: September 12, 2024
Revision Requested: March 3, 2025
Last Revision Received: February 26, 2025
Accepted: April 29, 2025
Publication Date: May 14, 2025

DOI: 10.5152/electrica.2025.24198

Content of this journal is licensed under a Creative Commons Attribution-NonCommercial 4.0 International License.

ABSTRACT

This study introduces a model that adjusts the DC voltage output from PV panels through a Cuk Converter while a Class-E inverter produces a high-frequency AC voltage. The model addresses the impact of varying irradiation levels on the operational conditions of the PV panels. To counteract fluctuations in DC voltage due to temperature, irradiation, or load changes, a PI Controller is utilized to keep the DC voltage constant. This stable DC voltage is then converted to AC voltage at a frequency of 15 kHz using a Class-E inverter. This modeling study aimed to maintain the inverter's output voltage at a steady 100V (RMS), regardless of fluctuations in irradiation, temperature, and the load connected to the inverter. The modeling process involved testing four scenarios, with results analyzed for each. In the first scenario, variations in irradiation were managed effectively by the PI controller, which kept the output voltage constant. In the second scenario, when the panel temperature was modified, the PI controller ensured that the output voltage remained steady. The third scenario maintained a constant output load while altering the other two variables, and here, the PI controller successfully stabilized the output voltage as well. In the fourth scenario, all variables were changed together, dropping the output load below a critical level. As a result, the output voltage could not be kept constant due to inadequate irradiation. The study demonstrates that the model functions reliably within specific variable ranges, but instability occurs when multiple variables fall below acceptable levels simultaneously.

Index Terms— Class-E inverter, DC-AC voltage conversion, photovoltaic systems, PI controller

I. INTRODUCTION

Recently, the use of renewable energy sources in energy production has increased [1-4]. An important source of renewable energy is solar panels [5, 6]. The energy produced by solar panels vary directly depending on several factors, including solar radiation, the temperature of the panel, the angle between the panel and the incoming radiation, and weather conditions [7, 8]. Numerous studies have focused on the highest power output and characteristic curves of solar panels [8, 9]. In addition to keeping the produced energy at the highest level, converting it into the required form of energy is necessary. This requirement is accomplished through a direct current-direct current (DC-DC) converter, which links the load and the module. Direct current-direct current converters are particularly suitable for applications that require an average output voltage, which can be higher or lower than the input voltage. There are two main types of DC-DC converters: isolated and non-isolated [1, 10]. Examples of isolated converters are push-pull, reversing, forward, bridge, and resonant converters. On the other hand, commonly used non-isolated converters consist of buck, boost, buck-boost, Cuk, Luo, and single ended primary inductor converter (SEPIC) converters. The Cuk Converter is often preferred for adjusting the voltage level in these converters. The Cuk Converter can increase or decrease the voltage generated by the solar panel. It is often preferred due to its simple structure. The DC-DC conversion of energy acts as a pre-conversion in areas where DC-AC conversion is needed. When alternating current (AC) voltage is desired to be generated, a DC-AC converter must be added to the DC-DC converter output. Direct current-alternating current converters can be

- *Cuk Converters are widely used in PV systems due to their ability to both step up and step down voltage efficiently, offering advantages over buck, boost, and buck-boost converters in terms of continuous current and reduced ripple.*
- *Class-E inverters are recognized for their high efficiency and low switching losses in low-power applications, especially when operated at high frequencies with constant load conditions, although they exhibit sensitivity to load variations without proper regulation.*

listed under main headings such as Full Bridge Inverters, Half Bridge Inverters, and Resonance Inverters. Inverters with this structure have many power switches and high switching losses. In addition, the increasing number of power switches brings cost increases and design challenges. The output voltage frequency is also limited depending on the inverter structure. In the design of a high-frequency inverter, several challenges arise. The Class-E inverter topology comes to the fore to eliminate all these disadvantages. In this topology, using a single power switch significantly reduces switching losses. In this topology, which has a theoretical efficiency of 100%, high-frequency sinusoidal voltage can be generated [11, 12]. The major disadvantage of this topology is that high-power applications cannot be realized. It is ideal for a low-power, high-frequency inverter design.

This study is a model in which the DC voltage level obtained from photovoltaic (PV) panels can be adjusted with a Cuk Converter, and a high-frequency AC voltage can be obtained using a Class-E inverter. In the model, the variable irradiation that affects the operating conditions of the PV panels and the changing DC voltage level in temperature situations is kept constant with a Proportional-Integral (PI) Controller. The resulting constant DC voltage is converted into AC voltage with a frequency of 15 kHz using a Class-E inverter. The block diagram of the model is given in Fig. 1.

II. MATERIALS AND METHODS

The system is made up of three primary components and a controller. First, a PV array, which changes based on irradiation and temperature, acts as the voltage source. The DC voltage the PV array generates is fed into a Cuk converter, which a PI controller governs. This controller maintains a consistent output voltage from the Cuk converter at the specified level. The resulting stable DC voltage is then supplied to a Class-E inverter, where it is transformed into high-frequency AC. Comprehensive details about each component will be provided in the subsequent sections.

A. PV Array

The equivalent circuit topology of a PV panel is given in Fig. 2. The behavior of the PV panel varies according to irradiation (G) and temperature (T). Depending on these variables, electrical quantities can be calculated.

The model has derived the normalized working temperature (T_0) using (1).

$$T_0 = 273 + 25 \tag{1}$$

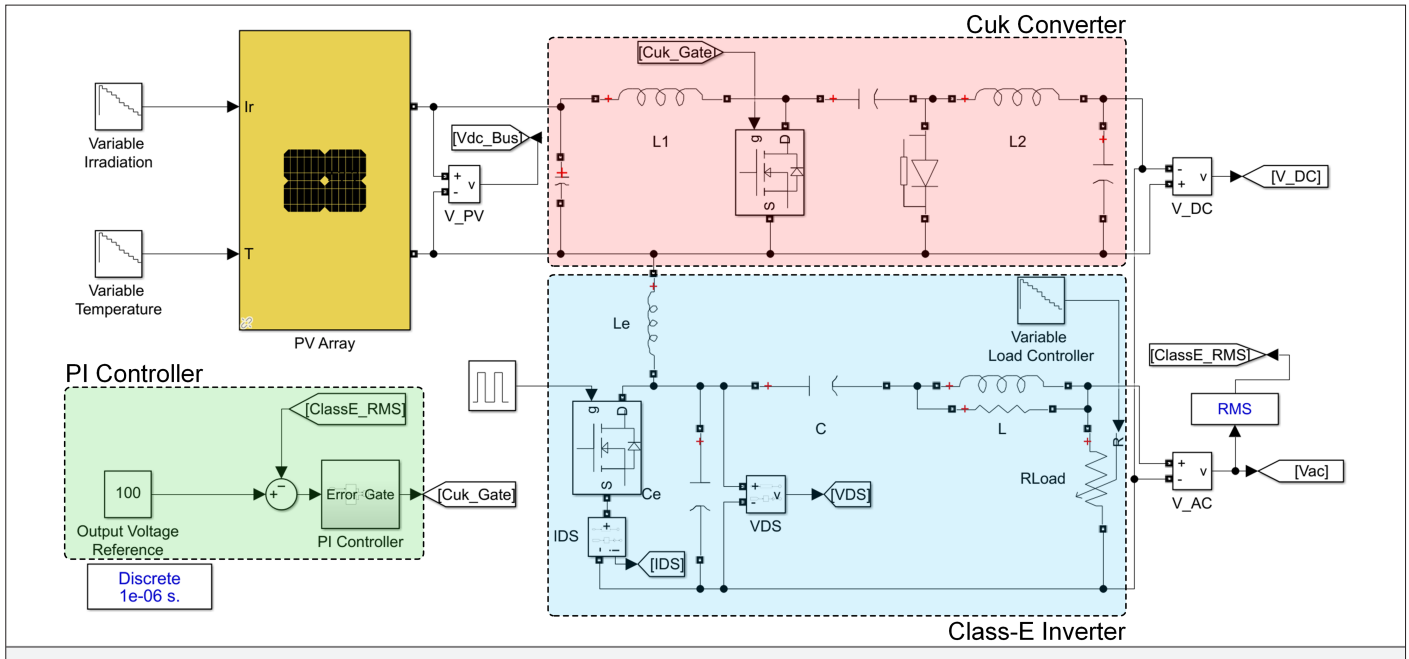

Fig. 1. Block diagram of the model.

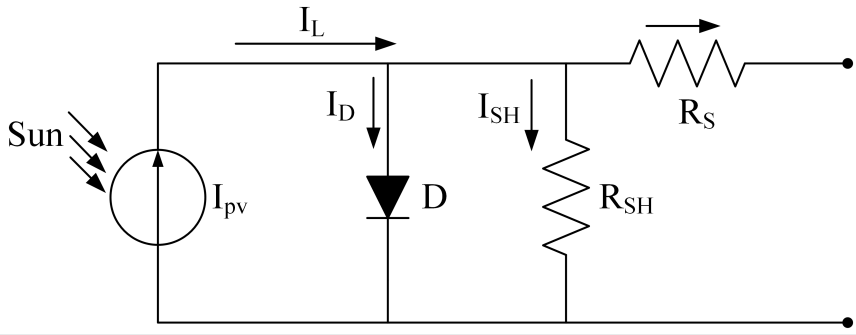

Fig. 2. Equivalent circuit topology of a PV panel.

Equation (2) was employed to calculate the panel's working temperature (T_K). This approach collected the panel's operating characteristics across different temperature levels.

$$T_K = 273 + T_C \tag{2}$$

The effect of radiation on panel current (I_{LT0}) has been calculated using (3) and then divided by 1000 to determine the sun's number. According to the literature, the association between radiation and sun number is 1 Sun = 1000 W/m².

$$I_{L_{T0}} = I_{Sc_{T0}} \frac{Irr}{1000} \tag{3}$$

The connection between photocurrent (I_L) and temperature is defined using (4). In this context, "K_0" refers to the current-temperature coefficient of the panel.

$$I_L = I_{L_{T0}} + K0\left(T_K - T_0\right) \tag{4}$$

The diode's saturation current (I_0) can be determined using (5). In this equation, "q" refers to the charge of an electron (C), "V_g" indicates the panel's raw material voltage (V), "n" represents the quality factor of the diode, and "k" stands for the Boltzmann constant (J/K).

$$I_0 = \left(\frac{I_{Sc_{T0}}}{e^{\frac{qV_{oc}(T_0)}{nkT_0}} - 1} \right) \left(\frac{T_K}{T0} \right)^{\frac{3}{n}} \left(e^{\frac{qV_g(T_0)}{nk\left(\frac{1}{T} - \frac{1}{T_0}\right)}} \right) \tag{5}$$

The module's open-circuit voltage is X_V, with I_{sc} and V_{oc} representing each cell's short-circuit current and open-circuit voltage.

$$XV = I_{0_{T0}} \frac{q}{nkT_0} e^{\frac{qV_{oc}(T_0)}{nkT_0}} \tag{6}$$

The panel's serial resistance effect (R_s) is determined by (7).

$$R_s = -\frac{dV}{dI_{V_{oc}}} - \frac{1}{X_V} \tag{7}$$

The instantaneous current of the panel is calculated using the previously mentioned variables. A parallel diode is incorporated to ensure the curves match as closely as possible. The output current (I_a) is derived using (8). In this equation, "V_a" stands for the panel's open-circuit voltage, and "V_t" refers to the thermal voltage (V) of the panel.

$$I_a = I_a - \frac{I_L - I_a - I_0\left(e^{\frac{V_a + I_a R_s}{V_t}} - 1 \right)}{\left(-1 - \left(I_0 \left(e^{\frac{V_a + I_a R_s}{V_t}} - 1 \right) \frac{R_s}{V_t} \right) \right)} \tag{8}$$

The provided equations were solved using the Newton–Raphson method.

B. Cuk Converter

The Cuk converter is a configuration that combines a boost converter and a buck converter in a sequential arrangement. It has numerous advantages over other types of converters, including buck, boost, and buck-boost converters [13]. Although the buck-boost converter is usually more affordable, it suffers from issues such as discontinuous input current and pulsating output current, resulting in a poorer transient response. The Cuk converter, on the other hand, has attributes that differ from those of the buck-boost converter and includes capacitive isolation, which helps to prevent switch failures. Figure 3 shows the circuit topology of the Cuk converter.

It does not provide the necessary steep step-up or step-down voltage for many applications. To achieve a high voltage conversion ratio, the converter must operate at a higher duty cycle, requiring the control circuit to have a quicker comparator. However, operating at elevated switching frequencies can increase the risk of control circuit failure, primarily due to the brief conduction time of the diode.

The parameters of the Cuk Converter must be calculated within certain limits. In (9), the conversion ratio D is calculated depending on the output voltage (V_{DC}) and input voltage (V_{PV}).

$$D = \frac{V_{DC}}{V_{DC} - V_{PV}} \tag{9}$$

Converter coils (L_1, L_2) in (10, 11) are dependent on the conversion ratio D and the switching frequency f.

$$L_1 = \frac{V_{DC} D}{\Delta i_{L1} f} \tag{10}$$

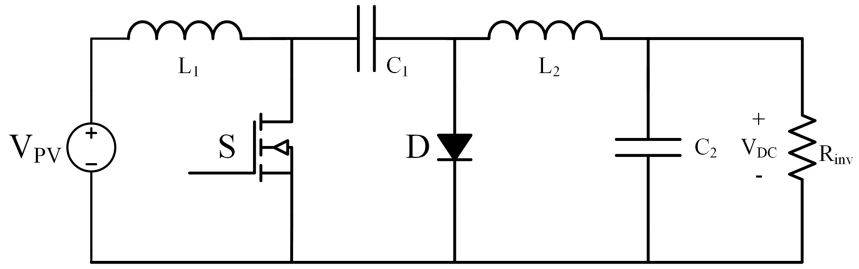

Fig. 3. Cuk converter circuit topology.

$$L_2 = \frac{V_{DC} D}{\Delta i_{L2} f} \tag{11}$$

Converter capacitors (C_1, C_2) are calculated in (12, 13).

$$C_1 = \frac{D}{R_{inv}\left(\frac{\Delta V_{C1}}{V_{DC}}\right) f} \tag{12}$$

$$C_2 = \frac{D}{R_{inv}\left(\frac{\Delta V_{DC}}{V_{PV}}\right) f} \tag{13}$$

C. Class-E Inverter

The Class-E inverter is highly efficient in converting power, demonstrating low sensitivity to changes in components, and is characterized by a straightforward circuit design [14]. In these inverters, the switch operates in an on-off mode, which helps prevent high current and voltage from impacting the switch along the load line. This operation facilitates the shaping of the output current and voltage waveforms [15]. This approach significantly reduces power loss, especially during the switching process. Class-E inverters feature a single-switch structure that results in low switching losses when operating under a constant load, offering a considerable advantage [16]. A key drawback of Class-E inverters is that they cannot sustain a steady load voltage when the load varies, making load regulation essential. To overcome this challenge, it is vital to create a mathematical model of the inverter and establish the key parameters and constraints required for effective regulation. The circuit design of the Class-E inverter is depicted in the diagram provided in Fig. 4.

In this circuit, V_{DC} indicates the source voltage, L_e signifies the inverter's input coil, S refers to the power switch metal oxide semiconductor field effect transistor (MOSFET), C_e represents the parallel capacitor, R_L is the load at the inverter's output, and C_{res} and L_{res} are parts of the resonance tank. The parallel capacitance comprises the parallel capacitor C_e and the parasitic capacitance at the MOSFET's output [17]. The resonant tank coil L_{res} is combined with the transmitter coil, removing the necessity for extra coils. The inverter's components and parameters are determined based on the chosen switching frequency and a duty cycle ratio of 50% [18]. The input voltage of the inverter is calculated using (14).

$$V_{DC} = \sqrt{\frac{R_L\left(\pi^2 + 4\right) P_o}{8}} \tag{14}$$

The input resistance of the inverter can be determined with the (15) shown below:

$$R_i = \frac{\left(\pi^2 + 4\right)}{8} R_L \tag{15}$$

The total current supplied by the source is illustrated in (16) and is a function of the input voltage and load resistance.

$$I_1 = \frac{8}{\pi^2 + 4} \frac{V_{DC}}{R_L} \tag{16}$$

Additionally, the amount of current supplied by the source sets the upper limit for the current that can pass through the power switch. This is an essential consideration in the process of choosing power switches [15]. The maximum current for the power switch can be calculated using the formula in (17).

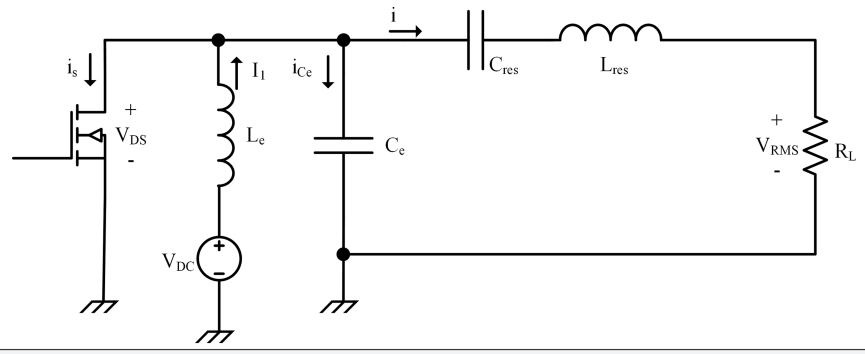

Fig. 4. Topology of class E inverter circuits.

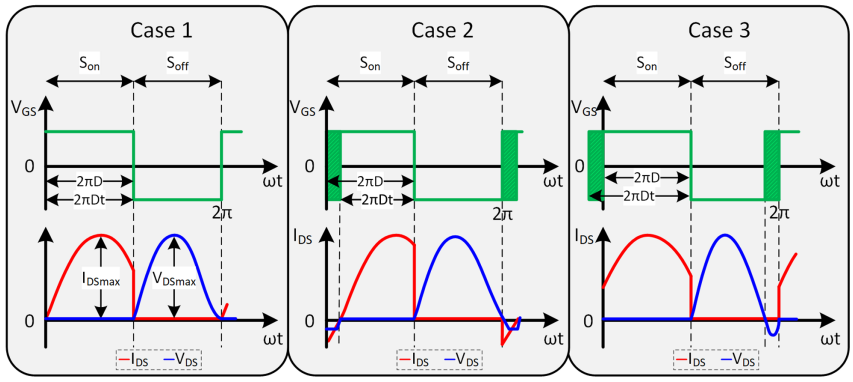

Fig. 5. Class-E inverter zero voltage switching operating states: a) case 1, b) case 2, and c) case 3.

$$I_{SM}=\left(\frac{\sqrt{\left(\pi^2+4\right)}}{2}+1\right)I_1 \tag{17}$$

The optimal operating case for the inverter is shown in Fig. 5, especially in case 1, where the switch voltage and its derivative must be zero during the transition to transmission mode. Component values are determined based on load resistance, and optimal performance occurs only at a specific value. If the load resistance is too high, the current through the resonant circuit will be inadequate. In case 2, the voltage across the C_e capacitor decreases, with a positive switch voltage at switching. In case 3, if the load resistance is too low, the current will exceed optimal levels, causing the C_e capacitor voltage to increase and the switch voltage to become negative.

In cases where load match is not achieved, the values of the circuit components must be adjusted. In the circuit, increasing the value of the capacitor C_e moves the groove formed at the switch voltage up and to the right. Increasing the value of the C_{res} capacitor moves the groove down and to the right. Increasing the L_{res} value moves the groove down and to the right. Increasing the load resistance moves the groove upwards and decreases it downwards. The situation in which inverter load compatibility is achieved and the effect of circuit components on V_{DS} voltage are given in Fig. 6.

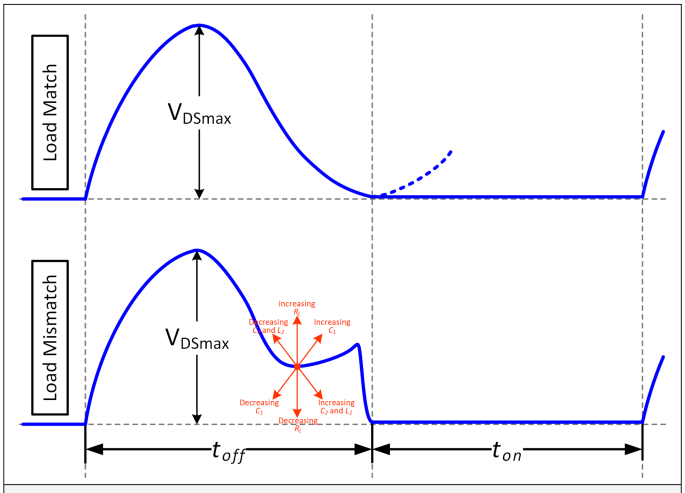

Fig. 6. Effect of circuit components on load matching.

D. PI Controller

A fundamental element of closed-loop control systems is the PI controller, which is essential for numerous applications in power electronics. The mathematical formulation of PI control, a linear control method, is described in (18). Kp refers to the proportional gain in this framework, and K_i represents the integral gain. *F(t)* refers to the control signal, and *e* indicates the error.

$$F(t)=K_p e(t)+K_i\int e(t)d(t) \tag{18}$$

The PI controller compares the input signal to the output feedback, generating an error that reflects the difference between the two signals, as shown in Fig. 7. In response, the controller aims to minimize this error and sends the adjusted output accordingly. Continuous feedback from the output to the input helps identify the errors. This cycle continues until the error is reduced. The controller's impact on the output serves to decrease the error. This method is highly favored because of its straightforward mathematical model and the minimal number of parameters that need adjustment [19]. In the study, the PI Controller parameters were optimized using MATLAB PID AutoTuner and set to $K_p = 0.15$, $K_i = 10.33$.

III. RESULTS AND DISCUSSION

In the modeling study, it was desired to keep the inverter output voltage constant at 100V (RMS) according to the change of Irradiation and Temperature, which are the variables of PV panels, and according to the change of the inverter output load. In the first study, the PV panel temperature and output load were kept constant, and the Irradiation value was changed in the range of 100–800W/m² with 1s periods. Except for the initial situation, it was observed that the Inverter output voltage for 11 different Irradiation values was kept constant by the PI Controller at the target voltage value of 100V (RMS). The results of the first modeling study are presented in Fig. 8.

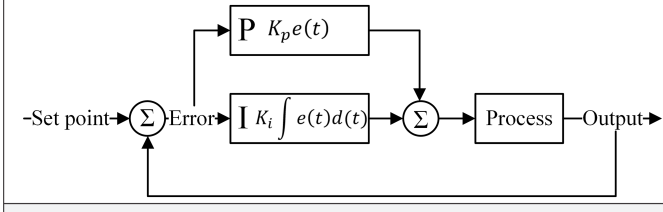

Fig. 7. Block diagram of PI controller.

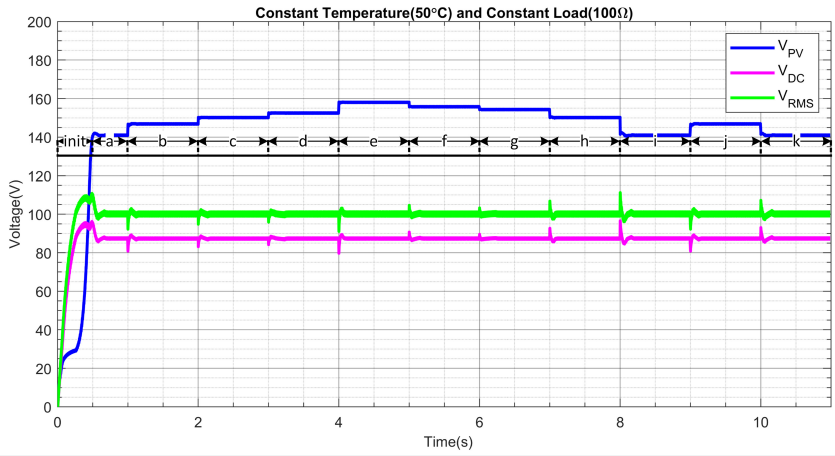

Fig. 8. Modeling results under constant temperature, constant load, and variable irradiation conditions.

In this case, where the output voltage can be kept constant, the voltage falling on the inverter power switch is given in $V_{DS,}$ and the switch current I_{DS} is shown in Fig. 9(a) and (b). In this case, where the output load directly affects the switch voltage and current, it has been observed that the switch voltage and current remain constant. Under these conditions, the power switch operates in zero voltage switching (ZVS) and a safe zone.

In the second modeling study, PV irradiation and output load were kept constant, and the panel temperature value was changed at

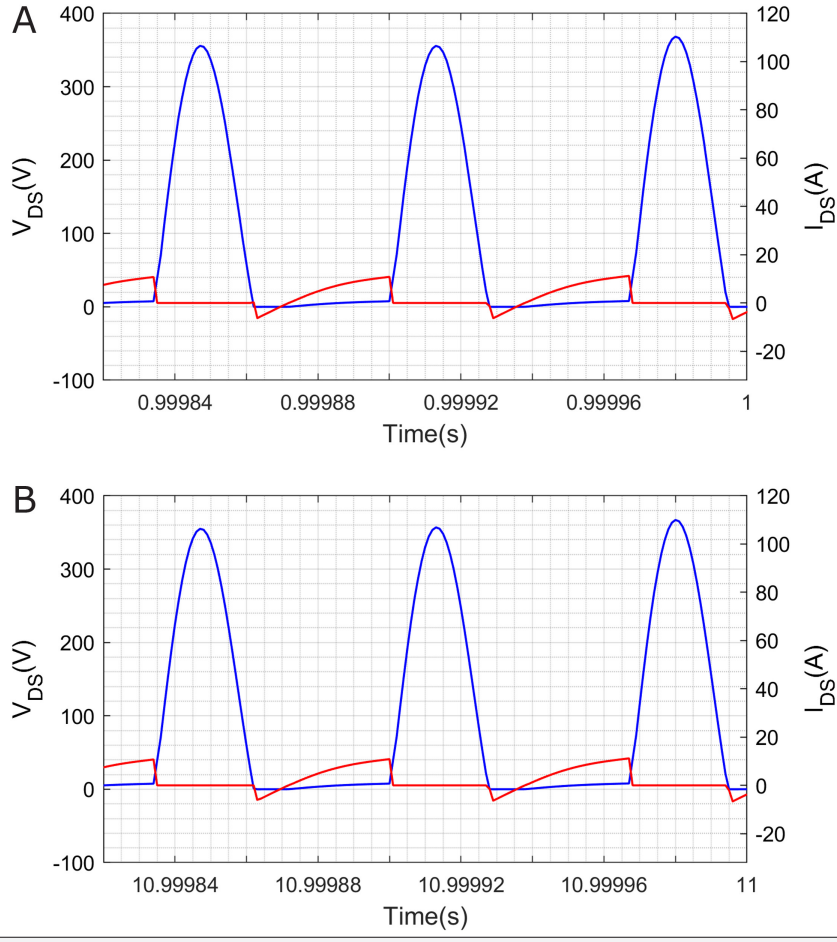

Fig. 9. a. Switch voltage and current for constant temperature at initial conditions. b. Switch voltage and current for constant temperature at end conditions.

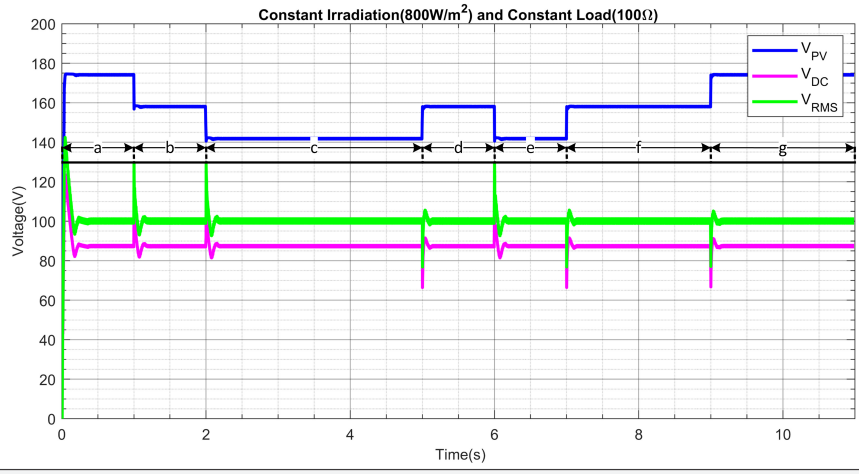

Fig. 10. Modeling results under constant irradiation, constant load, and variable temperature conditions.

1-second intervals in the range of 25°–75°C. Except for the initial situation, it was observed that the Inverter output voltage for seven different temperature values was kept constant by the PI Controller at the target voltage value of 100V (RMS). The results of the second modeling study are presented in Fig. 10.

In this situation, where the output voltage can be maintained at a constant level, the voltage across the inverter power switch is expressed as V_{DS}. In contrast, the switch current I_{DS} is represented in Fig. 11(a) and (b). In this scenario, since the output load directly influences the switch's voltage and current, it has been noted that

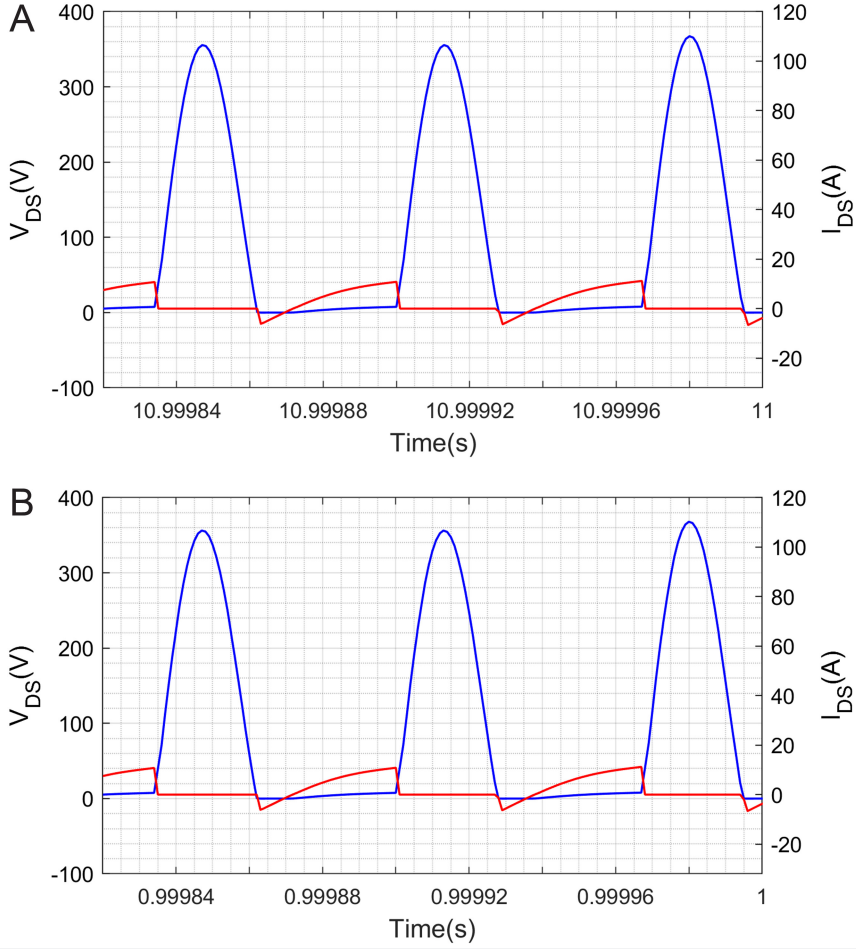

Fig. 11. a. Switch voltage and current for constant irradiation at initial conditions. b. Switch voltage and current for constant irradiation at end conditions.

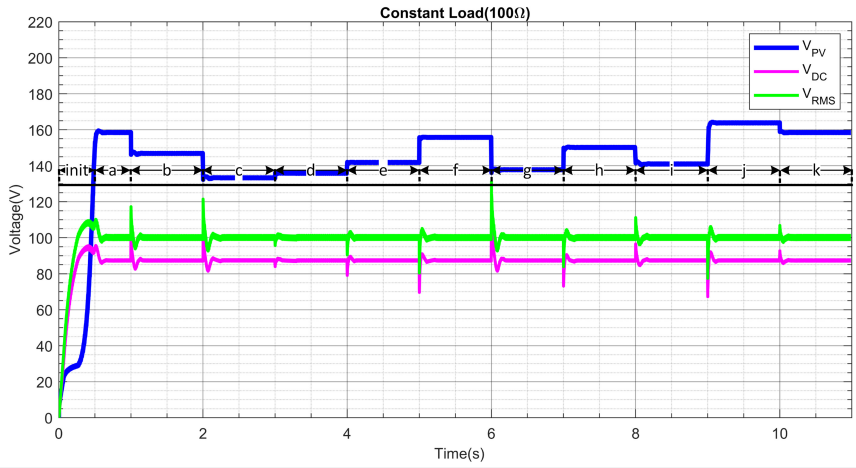

Fig. 12. Modeling results under constant load, variable irradiation, and variable temperature conditions.

both the switch voltage and current stay constant. Under these circumstances, the power switch functions with ZVS and is in a safe operating zone.

In the third modeling study, only the output load was kept constant, the Panel Temperature value was changed in the range of 25°–75°C, and the Irradiation value was changed in the range of 100–800W/m^2 with 1-second periods. Except for the initial situation, it was observed that the Inverter output voltage for 11 different Irradiation and Temperature values was kept constant by the PI Controller at the target voltage value of 100V (RMS). The results of the third modeling study are presented in Fig. 12.

In the last modeling study, the output load was changed in the range of 5–50Ω, the Panel Temperature value in the range of 25°–75°C, and the Irradiation value in the range of 100–800W/m^2 with 1-second periods. Except for the initial state, it was observed that the Inverter output voltage for 11 different Load, Irradiation, and Temperature values was kept constant by the PI Controller at the target voltage value of 100V (RMS), except for 3 cases shown as *a, i, and j* in Fig. 13. For these 3 cases, the Panel approached the short-circuit voltage at the low load value, and the PI Controller could not raise the voltage.

In this case, which is different from other scenarios, the variable in the inverter load directly changes the inverter voltage and current. The change of the inverter load changes the voltage falling on the switch and can eliminate the ZVS conditions of the inverter. For this scenario, the key voltage and current graphs obtained in 11 different variable states are given in Fig. 14(a) and (b).

The graphs in Fig. 14(a)-(h) show that the switch voltage increased as the load resistance decreased. The increase in the switch voltage increases the switching losses and can cause the switch to move out of the safe operating zone. In (i) and (k), the switch continues to operate in the safe zone as in the previous scenarios. In case (j), the switch voltage has increased excessively, and the key safety has reached the point where the switch's security has become dangerous. In this case, it should be noted that switching losses also increase.

IV. CONCLUSION

In the modeling study, it was desired to fix the inverter output voltage to 100V (RMS) according to the change of Irradiation and Temperature, which are the variables of PV panels, and according to the change of the inverter output load. Modeling was carried out for four situations, and the results were evaluated. For the first case, with

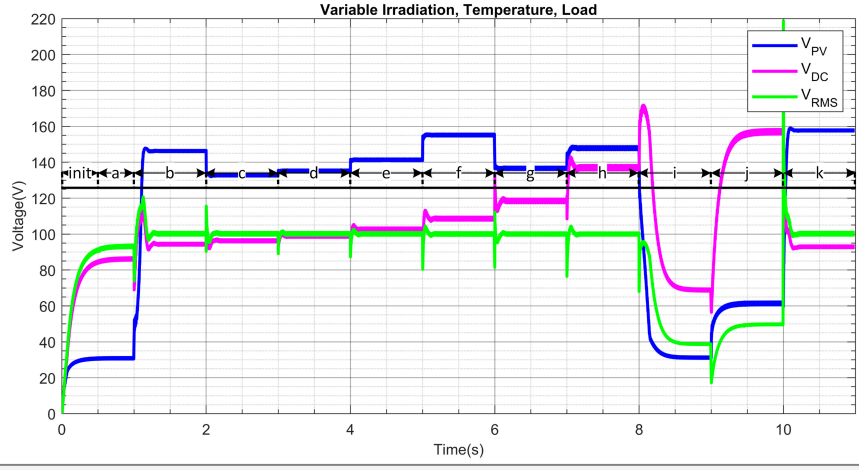

Fig. 13. Modeling results under variable load, variable irradiation, and variable temperature conditions.

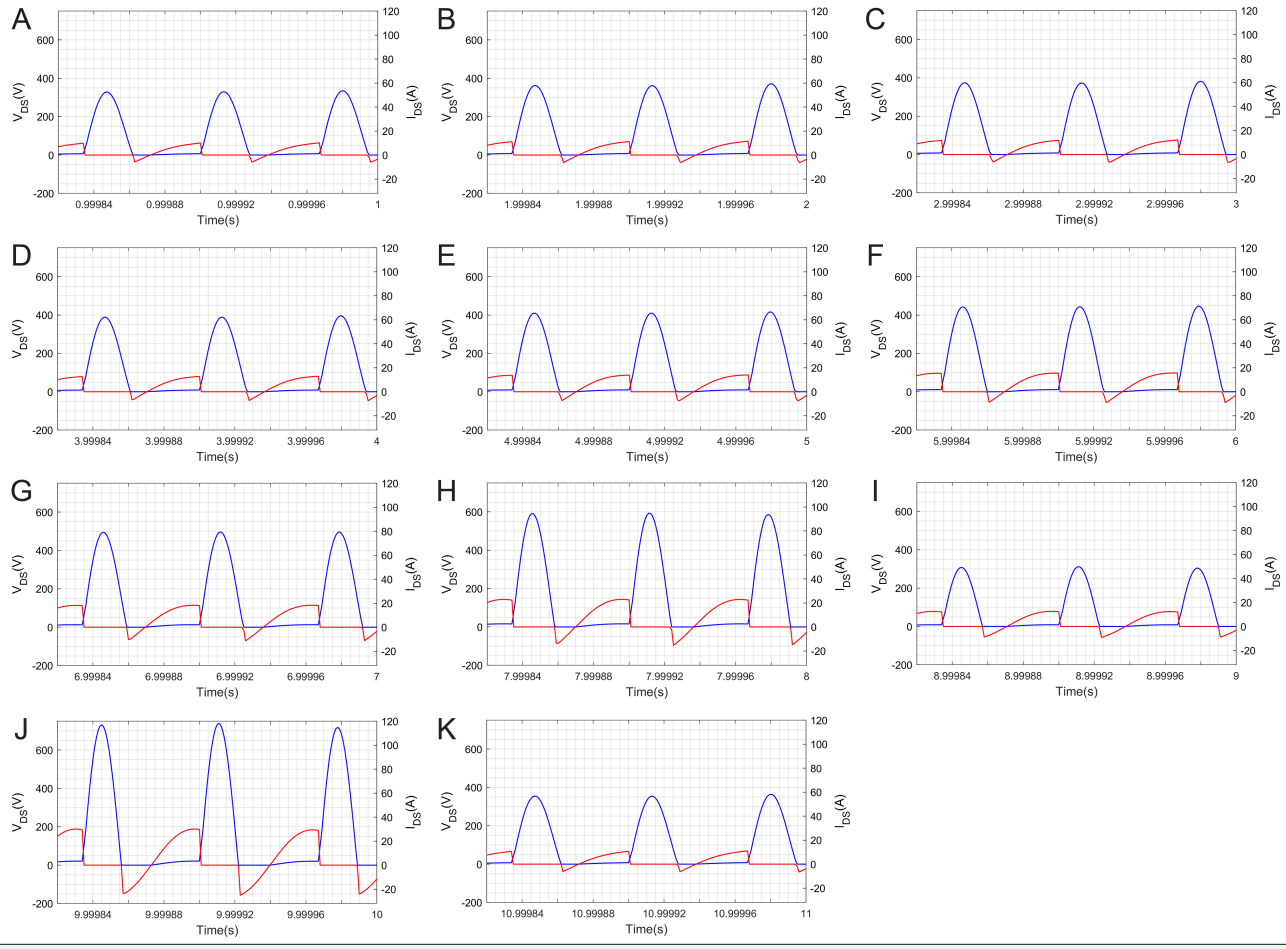

Fig. 14. a. Switch voltage and current at end condition of (a). b. Switch voltage and current at end condition of (b). c. Switch voltage and current at end condition of (c). d. Switch voltage and current at end condition of (d). e. Switch voltage and current at end condition of (e). f. Switch voltage and current at end condition of (f). g. Switch voltage and current at end condition of (g). h. Switch voltage and current at end condition of (h). i. Switch voltage and current at end condition of (i). j. Switch voltage and current at end condition of (j). k. Switch voltage and current at end condition of (k).

the variable irradiation value, the PI controller ensured that the output voltage was kept constant. In the second case, the panel temperature was changed, and again, it was observed that the PI controller kept the output voltage constant. In the third case, only the output load was kept constant while the other two variables were changed. In this case, the PI controller successfully kept the output voltage constant. In the last case, all variables were changed, and modeling results were obtained. This situation caused the output load value to fall below a certain level, and the output voltage could not be kept constant due to the same low irradiation value. It has been observed that the modeling study works stably within certain variable ranges, and if more than one variable is insufficient simultaneously, it causes instability.

Data Availability Statement: The data that support the findings of this study are available on request from the corresponding author.

Peer-review: Externally peer-reviewed.

Author Contributions: Concept – F.I., M.K.; Design – F.I., M.K.; Supervision – F.I., M.K.; Resources – F.I., M.K.; Materials – F.I., M.K.; Data Collection and/or Processing – F.I., M.K.; Analysis and/or Interpretation – F.I., M.K.; Literature Search – F.I., M.K.; Writing Manuscript – F.I., M.K.; Critical Review – F.I., M.K.

Declaration of Interests: The authors have no conflict of interest to declare.

Funding: The authors declared that this study has received no financial support.

REFERENCES

1. M. Zhou, C. Liu, R. Xie, Y. Zhuang, X. Mao, and Y. Zhang, "A high-gain Three-Port DC-DC converter with soft-switching for renewable energy system applications," *IEEE Trans. Power Electron.*, vol. 40, no. 1, pp. 1508–1518, 2025. [CrossRef]
2. F. N. Oppong, H. F. Ahmed, A. A. Khan, and J. E. Quaicoe, "High-gain single-stage single-phase common-ground buck-boost inverter," *IEEE Trans. Power Electron.*, vol. 40, no. 1, pp. 1074–1084, 2025. [CrossRef]
3. J. Ma et al., "Improving power-conversion efficiency via a hybrid MPPT approach for photovoltaic systems," *Electron. Elektrotech.*, vol. 19, no. 7, pp. 57–60, 2013. [CrossRef]
4. S. Borekci, E. Kandemir, and A. Kircay, "A simpler single-phase single-stage grid-connected PV system with maximum Power Point tracking controller," *Electron. Elektrotech.*, vol. 21, no. 4, pp. 44–49, 2015. [CrossRef]
5. V. Karthikeyan, G. Vijaysaikumar, B. Sumanthreddy, G. Abhilash, S. B. A. S. Ali, and B. Ramkiran, "Performance analysis of the standalone photovoltaic system," in 2017 Third International Conference on Advances in Electrical, Electronics, Information, Communication and Bio-Informatics (AEEICB), 27-28 Feb, 2017, pp. 486–490. [CrossRef]

6. A. Procházka, J. Švihlík, H. Charvátová, and V. MAříK, "Advanced signal processing techniques for monitoring East/West oriented solar photovoltaic systems: A case study," *IEEE Access*, vol. 12, pp. 165042–165049, 2024. [CrossRef]
7. M. Belik, "Simulation of photovoltaic panels thermal features," in 2017 18th International Scientific Conference on Electric Power Engineering (EPE), 17-19 May, 2017, pp. 1–5. [CrossRef]
8. N. Tavakoli, P. Koelblin, and M. Saliba, "Design and development of a new smart portable I-V Tracer," *IEEE J. Photovolt.*, vol. 14, no. 6, pp. 951–959, 2024. [CrossRef]
9. O. Kaplan, F. Issi, and M. Ersan, "A high efficient driver design for LED lighting system," in International Conference on Power Engineering, Energy and Electrical Drives, 2013, pp. 1548–1552. [CrossRef]
10. S. Hadji, A. Belkaid, K. Kayisli, I. Colak, S. Aissou, and L. Larbi, "A comparative analysis of Cuk, SEPIC, and zeta converters as maximum Power Point trackers," in 2024 12th International Conference on Smart Grid (icSmartGrid), 27-29 May, 2024, pp. 539–544. [CrossRef]
11. J. Ponte, A. Ghahremani, M. Huiskamp, A. J. Annema, and B. Nauta, "Theory and implementation of a load-mismatch protective class-E PA system," *IEEE Trans. Circuits Syst. I*, vol. 67, no. 2, pp. 369–377, 2020. [CrossRef]
12. K. Shinde, and H. Koizumi, "Capacitive power transfer system using a load-independent Class E zero voltage switching parallel resonant inverter and a Class D voltage-driven rectifier," *IEEE Trans. Circuits Syst. II*, vol. 71, no. 9, pp. 4366–4370, 2024. [CrossRef]
13. S. Samantara, B. Roy, R. Sharma, S. Choudhury, and B. Jena, "Modeling and simulation of integrated CUK converter for grid connected PV system with EPP MPPT hybridization," in 2015 IEEE Power, Communication and Information Technology Conference (PCITC), 15-17 Oct., 2015, pp. 397–402. [CrossRef]
14. R. Zulinski, "A high-efficiency self-regulated class E power inverter/converter," in *IEEE Trans. Ind. Electron.*, vol. 33, no. 3, pp. 337–344, 1986. [CrossRef]
15. N. O. Sokal, "*Class-E RF Power Amplifiers*", QEX, no. 204, pp. 9–20, 2001.
16. A. Lotfi et al., "Subnominal operation of Class-E nonlinear shunt capacitance power amplifier at any duty ratio and grading coefficient," *IEEE Trans. Ind. Electron.*, vol. 65, no. 10, pp. 7878–7887, 2018. [CrossRef]
17. A. Ayachit, F. Corti, A. Reatti, and M. K. Kazimierczuk, "Zero-voltage switching operation of transformer Class-E inverter at any coupling coefficient," *IEEE Trans. Ind. Electron.*, vol. 66, no. 3, pp. 1809–1819, 2019. [CrossRef]
18. D. C. Marian, and K. Kazimierczuk, *Resonant Power Converters*, 2nd ed. Chichester, UK: John Wiley & Sons, 2011.
19. S. Vadi, F. B. Gurbuz, S. Sagiroglu, and R. Bayindir, "Optimization of PI based buck-boost converter by particle swarm optimization algorithm," in 2021 9th International Conference on Smart Grid (icSmartGrid), 29 June–1 July, 2021, pp. 295–301. [CrossRef]

Fatih ISSI received the B.Sc. and M.Sc. degrees in electrical education from Gazi University, Ankara, Turkey, in 2011 and 2013, respectively. He received a Ph.D. in electrical and electronic engineering from Gazi University in 2021. He worked in the Department of Electronics and Automation, Cankiri Karatekin University, Turkey, from 2013 to 2025. He works as an Associate Professor in the Computer Engineering Department at Çankırı Karatekin University. His research interests include wireless power transfer, high-frequency power inverters, energy conversion, and machine-learning applications for power electronics.

Mustafa Karhan received his Ph.D. degree in Electrical and Electronics Engineering from Istanbul University, Türkiye, in 2017. From 2008 to 2012, he worked as a Research Assistant in the Electronics and Communication Engineering Department at Namık Kemal University. From 2012 to 2013, he worked as a Lecturer in the Electronics and Automation Department at Bingöl University. From 2013 to 2022, he worked as a Lecturer in the Electronics and Automation Department at Çankırı Karatekin University. He is currently working as an Associate Professor in the Computer Engineering Department at Çankırı Karatekin University. His research interests include image processing, machine learning, signal processing, the aging of polymeric insulators, dielectric materials, high voltage, dielectric phenomena, and wettability behavior.